Measurement of angular and momentum distributions of charged particles within and around jets with the ATLAS detector

M. Krivos, on behalf of the ATLAS Collaboration[i]

Charles University, Prague.

Studies of jet fragmentation in heavy-ion collisions can provide information about the mechanism of jet quenching inside the hot and dense QCD matter created in these collisions. These proceedings present results from measurements of charged particle yields within and around the jets in dijet, gamma+jet and Z+jet systems measured in 5.02 TeV Pb+Pb and pp collisions using the ATLAS detector at the LHC.

1. Introduction

In the collisions of the ultrarelativistic heavy nuclei at the Large Hadron Collider (LHC), hot and dense matter called a quark-gluon plasma QGP (see Refs. [1,2] for recent reviews) is produced. Jets from hard-scattering processes traverse and interact with this medium. During that, they lose energy via a process called jet quenching. The rates and characteristics of these jets in heavy-ion collisions can be compared with the same quantities in pp collisions, where no production of QGP is expected. The comparison between pp and heavy-ions can give valuable information about the properties of the QGP and its interaction with partons from the hard-scatterings. This proceeding refers to results measured by the ATLAS detector [3].

In the most central lead-lead (Pb+Pb) collisions at the LHC, jets with large transverse momenta, p_T^{jet}, are measured to have approximately one half of the rates in pp collisions when the nuclear overlap function of Pb+Pb collisions is taken into account [4-8]. Photon-jet pairs [9,10] and back-to-back dijet [11-13] are observed to have less-balanced transverse momenta in Pb+Pb collisions compared to pp collisions as well. In these measurements, it is suggested that part of the energy from hard-scattered parton is transferred outside of the jet via interactions with the strongly-interacting QGP medium.

Different, but complementary measurements are studying the modification of the jets structure in Pb+Pb collisions respectively to those in pp. Foregoing results have shown a broadening of jets in Pb+Pb [14-17] and an excess of low- and high-momentum charged particles as well. Depletion of the intermediate-momentum charged particles associate with these jets is also observed. Particles with a large fraction of the jet momentum are usually narrowly aligned with the axis of the jet. On the other hand, low-momentum particles are observed to have a much broader angular distribution extending outside the jet [12,18-21]. These results are suggesting that a process of soft gluon emission near the jet axis is responsible for the loss of the energy for jet quenching phenom-

ena [22-28]. Measuring yields of these particles with respect to angular distance between the particle and the jet axis and as a function of transverse momentum, p_T, may give more insight into the structure of jets after they have passed through the QGP and make a better understanding the the QGP itself.

2. Inclusive fragmentation functions

This proceeding picks the most important results from several papers quantifying p_T distributions of charged particles at a distance r around the jet axis. The measured yields which are corrected for the detector effect are defined as follows [29]:

$$D(p_T, r) = \frac{1}{N_{jet}} \frac{1}{2\pi r dr} \frac{dn_{ch}(p_T, r)}{dp_T},$$

where N_{jet} is the number of jets in consideration and $n_{ch}(p_T, r)$ is the number of charged particles with a given p_T at a distance r from the jet axis. The ratios of the charged-particle yields measured in Pb+Pb and pp collisions

$$R_{D(p_T, r)} = \frac{D(p_T, r)_{|Pb+Pb}}{D(p_T, r)_{|pp}},$$

quantify the modifications of the yields due to the QGP medium. Furthermore, the differences between the $D(p_T, r)$ distributions in Pb+Pb and pp collisions

$$\Delta D(p_T, r) = D(p_T, r)_{|Pb+Pb} - D(p_T, r)_{|pp},$$

allow the absolute differences in charged-particle yields between the two collision systems to be measured.

Generally, $D(p_T, r)$ distributions evaluated in pp and Pb+Pb collisions decrease as a function of distance from the jet axis. The rate of fall-off increases rapidly for higher p_T particles, with most of them being concentrated near the jet axis. The distributions shows a difference in shape between Pb+Pb and pp collisions, with the Pb+Pb distributions being broader at low p_T ($p_T < 4$ GeV) and narrower at high p_T ($p_T > 4$ GeV). This modification depends on the collision centrality and is smaller for more peripheral Pb+Pb collisions.
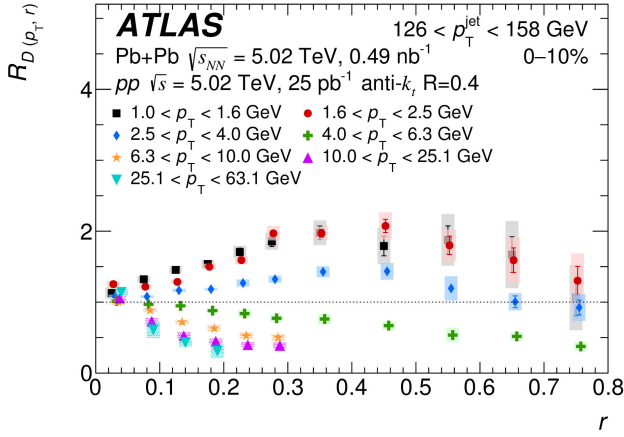
FIGURE 1. Ratio of $D(p_T, r)$ distributions in Pb+Pb to those in pp collisions as a function of angular distance r for $126 < p_T^{\text{jet}} < 158$ GeV for seven charged particles p_T selections. Only the most central collisions $0 - 10\%$ are shown. The vertical bars on the data points indicate statistical uncertainties, while the shaded boxes indicate systematic uncertainties. The widths of the boxes are not indicative of the bin size, and the points are shifted horizontally for better visibility. Figure from [29].

3. Radial dependency of fragmentation functions

To quantify modifications seen in $D(p_T, r)$ distributions, ratios of the $D(p_T, r)$ distributions in Pb+Pb collisions to those measured in pp are evaluated in charged particle p_T for seven bins in jet p_T and three bins in Pb+Pb centrality. $R_{D(p_T, r)}$ measured for $p_T^{\text{jet}} = 126 - 158$ GeV are show in Fig. 1.

In $0 - 10\%$ central collisions, $R_{D(p_T, r)}$ is greater than unity for approximately $r < 0.8$ for charged particles with p_T less than 4.0 GeV. For these particles, the enhancement of yields in Pb+Pb collisions compared to those in pp collisions grows with increasing r up to approximately $r = 0.3$, with $R_{D(p_T, r)}$ reaching values up to two for $1.0 < p_T < 2.5$ GeV. The values of $R_{D(p_T, r)}$ is approximately constant for r in the interval $0.3 - 0.6$ and for $r > 0.6$ is decreasing. For charged particles with $p_T > 4.0$ GeV, $R_{D(p_T, r)}$ is showing a depletion outside the jet core for $r > 0.05$. With increasing r up to $r = 0.3$ the magnitude of this depletion is increasing and is approximately constant thereafter. For more peripheral collisions, the enhancement in the yield of particles with $p_T < 4.0$ GeV is similar to those in the most central collisions, but the depletion is not as strong for particles with $p_T > 4.0$ GeV. There is no significant r dependence for $R_{D(p_T, r)}$ in the most peripheral collisions $(60 - 80\%)$ and the values of $R_{D(p_T, r)}$ are within approximately 50% of the unity. For more details see [29].

3.1. $\Delta D(p_T, r)$ distributions

To further quantify the modification in terms of the particle density, differences between the unfolded charged-particle
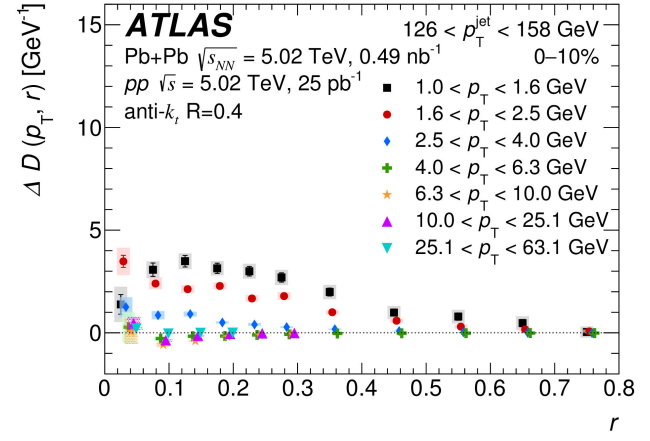
FIGURE 2. $\Delta D(p_T, r)$ as a function of r in central collisions for all p_T ranges for $126 < p_T^{\text{jet}} < 158$ GeV. The vertical bars on the data points indicate statistical uncertainties, while the shaded boxes indicate systematic uncertainties. The widths of the boxes are not indicative of the bin size, and the points are shifted horizontally for better visibility. Figure from [29].

yields are also evaluated as $D(p_T, r)$. Figure 2 shows these as a function or r for seven different charged particle p_T selections for $0 - 10\%$ centrality interval. Compared to pp collisions, the Pb+Pb distribution shows an excess in the charged-particle yield density for charged particles with $p_T < 4.0$ GeV, where the largest excess is being observed within the jet cone. Outside the jet cone, the difference decreases but remains positive.

3.2. Integrals of fragmentation functions

The unfolded $D(p_T, r)$ distributions are integrated for charged particles p_T in the interval of $1 - 4$ GeV to construct the quantity $\Theta(r)$:

$$\Theta(r) = \int\limits_{1\,\text{GeV}}^{4\,\text{GeV}} D(p_T, r)dp_T.$$

The new distribution provides a concise look at the p_T region of the enhancement discussed above and are compared between Pb+Pb and pp in term of:

$$\Delta_{\Theta(r)} = \Theta(r)_{\text{Pb+Pb}} - \Theta(r)_{pp},$$

$$R_{\Theta(r)} = \frac{\Theta(r)_{\text{Pb+Pb}}}{\Theta(r)_{pp}}.$$

Defined quantities are intended to provide aggregate information about the variation with angular distance from the jet axis, p_T^{jet} dependence of the low-p_T charged-particle excess and magnitude. The usefulness of the ratio quantities is also in the good possibility to compare with other Pb+Pb measurements.

In the Fig. 3 is shown the $\Delta\Theta(r)$ distributions for different p_T^{jet} selections for the centrality interval $0 - 10\%$. In these, a significant p_T^{jet} dependence on $\Delta\Theta(r)$ is observed; for the particles withing the jet cone $(r < 0.4)$ $\Delta\Theta(r)$ is increasing
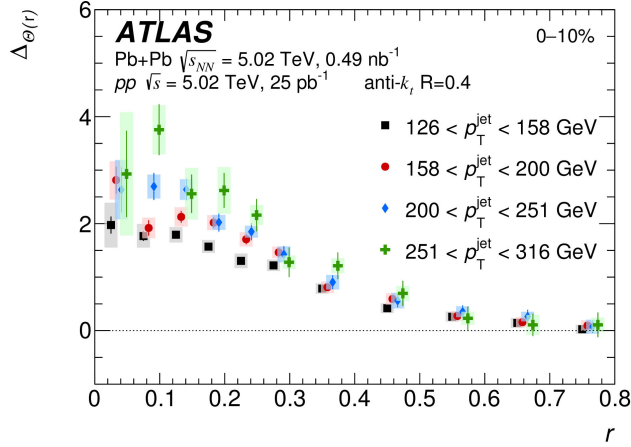
FIGURE 3. $\Delta\Theta(r)$ as a function of r for charged particles with $p_T < 4$ GeV in four p_T^{jet} selections: $126 - 158$ GeV, $158 - 200$ GeV, $200 - 251$ GeV, and $251 - 316$ GeV for centrality $0 - 10\%$. The vertical bars on the data points indicate statistical uncertainties, while the shaded boxes indicate systematic uncertainties. The widths of the boxes are not indicative of the bin size, and the points are shifted horizontally for better visibility. Figure from [29].
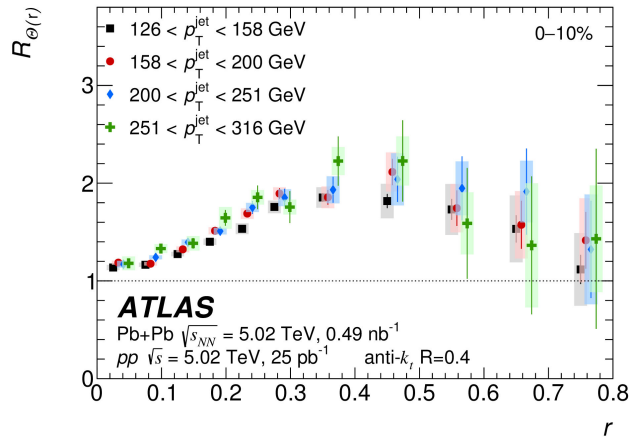
FIGURE 4. $R_{\Theta(r)}$ for charged particles with $p_T < 4$ GeV ranges in four p_T^{jet} selections: $126 - 158$ GeV, $158 - 200$ GeV, $200 - 251$ GeV, and $251 - 316$ GeV and centrality $0 - 10\%$. The vertical bars on the data points indicate statistical uncertainties, while the shaded boxes indicate systematic uncertainties. The widths of the boxes are not indicative of the bin size, and the points are shifted horizontally for better visibility. Figure from [29].

with p_T^{jet}. The value of $\Delta\Theta(r)$ decreases in more-peripheral collisions (not shown here), where its p_T^{jet} dependence is no longer significant.

Figure 4 shows $R_{\theta(r)}$ for the $0 - 10\%$ centrality interval for different jet p_T. A maximum for $r \sim 0.4$ is observed and a flattening or a decrease for larger r values, but never goes below the unity.

4. Gamma-jet systems

In the above measurement, jets are selected by their final p_T, *i.e.*, after the effects of quenching, which may result in a bias towards jets that have suffered only modest modifications and complicates interpretation of the data [27,30]. Alternatively, the initiating parton p_T can be tagged with a particle unaffected by the QGP medium, such as a photon [31-33]. The photon p_T approximately balances the parton p_T before quenching and, thus, selects populations of jets in pp and Pb+Pb collisions with identical initial conditions. A jet recoiling against a prompt photon is more likely to be initiated by the showering of a light quark, compared to inclusive jets where gluons are the initiators more frequently. Because of that, γ-tagged jets can provide information about how energy loss depends on the color charge of the initiating parton. While the inclusive selection may be biased towards jets which have lost less energy or were produced near the surface of the medium, the photon selection equally samples all geometric production points [34-36].

Figure 5 summarizes ratios of the γ-tagged fragmentation functions in Pb+Pb events to those in pp events, and compares them with those inclusively selected jets for p_T interval $p_T^{\text{jet}} = 100 - 126$ GeV measured in 2.76 TeV Pb+Pb and pp collisions [37]. Although the collision energy and p_T^{jet} range are not equal than that for the γ-tagged jet data, it was observed that the inclusive jet fragmentation functions in this region are compatible at the two energies and in nearby p_T^{jet} ranges within uncertainties [38]. Because of the difference in centrality ranges in the inclusive-jet measurement, the centrality range corresponding to the top of that in the γ-tagged measurement is chosen (*i.e.*, $0 - 10\%$ for $0 - 30\%$ in the case of γ-tagged, and $30 - 40\%$ for $30 - 80\%$). In the peripheral collisions, the modification shape is quantitatively similar for both sets of jets, observing a depletion at moderate z values and an enhancement at very low and very high z values. Nonetheless, in central collisions, γ-tagged jets show an +ad-
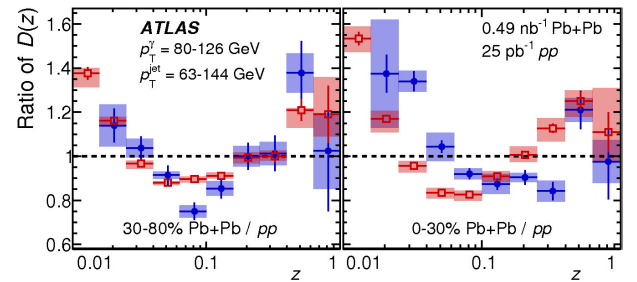
FIGURE 5. Ratio of the fragmentation function in jets azimuthally balanced by a high-p_T photon: $30 - 80\%$ Pb+Pb collisions to pp collisions (left); $0 - 30\%$ Pb+Pb collisions to pp collisions (central); and $0 - 30$ to $30 - 80\%$ Pb+Pb collisions (right) as a function of longitudinal momentum fraction z, for γ-tagged jets (full markers) and for inclusive jets in 2.76 TeV Pb+Pb collisions [37,39] (open markers). Hatched bands and vertical bars show for each measurement the total systematic and statistical uncertainties, respectively. Figure from [40].

ditional relative suppression at high z and a counterbalancing enhancement at low z. On top of that, the minimum value of the Pb+Pb-to-pp ratio for γ-tagged jets is shifted to larger z.

5. Z-tagged systems

Similarly to γ-tagged jets, Z boson can be used to mark the opposite jet p_T. At leading order, the Z boson and the jet are produced back to back in the azimuthal plane, with equal p_T. Because Z bosons and leptons (to which they decay), or similarly, photons, do not participate in the strong interaction, they are not modified by the QGP [41,42]. Because of that, they can provide an estimate of the p_T and azimuthal direction of the opposite hard-scattered parton before the developing jet shower is modified through interactions with the QGP [43,44].

To better reveal the modification, quantity I_{AA} is introduced, as the ratios of yields in Pb+Pb events to those in pp events:

$$I_{AA} = \frac{Y_{Pb+Pb}}{Y_{pp}},$$

where yields are defined as all charged particles opposite the Z boson in the chosen $\Delta\phi > 3/4\pi$ window. I_{AA} is suppressed at large p_T^{ch}, with a bigger suppression in more central events and for selection of lower p_T^Z. For $p_T^Z > 60$ GeV, the I_{AA} values at p_T^{ch} lower than $2-3$ GeV, are different compared to high p_T^{ch}, and is greater than unity. A similar increase at low p_T^{ch} is compatible with lower p_T^Z selections, although the uncertainties limit the significance of this enhancement. A qualitatively similar suppression is observed over a wide range of p_T^{ch} values, and the general enhancement of the I_{AA} above unity at lower p_T^{ch}, to those seen in the ratios of jet fragmentation functions in photon-tagged events [40].

Figure 5 compares the I_{AA} in $0-10\%$ Pb+Pb events with the following four theoretical calculations, which use the same kinematic selections as the data: (1) the Hybrid Strong/Weak Coupling model [34], which is combining initial production using PYTHIA8 with a parameterization of energy loss derived from holographic methods, including back reaction effects; (2) a perturbative calculation within the framework of soft-collinear effective field theory with Glauber gluons (SCETG) in the soft-gluon-emission (energyloss) limit, with jet-medium coupling $g = 2.0 \pm 0.2$ [46,47]; (3) a coupled linearized Boltzmann transport (COLBT) and hydrodynamics model [48,49], which includes jet-induced medium excitations; and (4) JEWEL, an MC event generator which simulates QCD jet evolution in heavy-ion collisions, including radiative and elastic energy loss processes, and configured to include medium recoils [36]. All metioned models qualitatively reproduce the magnitude of the degree of suppression at large p_T^{ch}, greater than 10 GeV. The Hybrid model, COLBT and JEWEL qualitatively describe the increase at low p_T^{ch}. For these three models, in this region, removing the backreaction, medium recoils, and jet-induced medium excitations, respectively, results in a significant un-
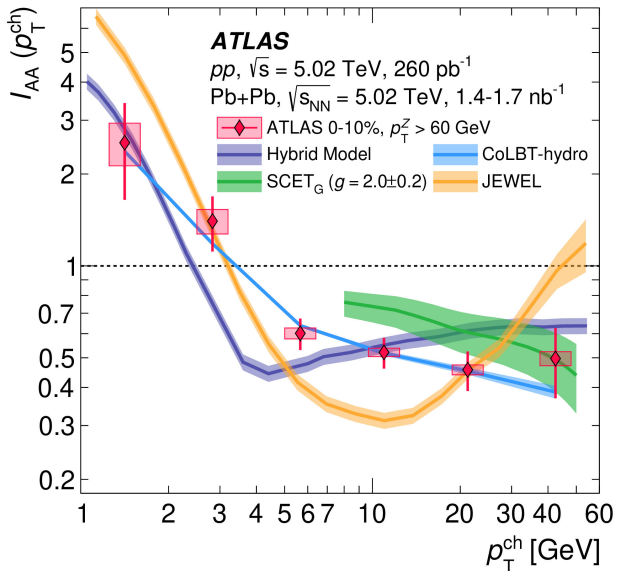
FIGURE 6. The I_{AA} ratio as a function of p_T^{ch} in data compared with theoretical simulations, for the selection $\Delta\phi > 3/4\pi$. The vertical bars and boxes correspond to the statistical and systematic uncertainties, while the shaded bands represent the theoretical uncertainty (statistical for JEWEL, Hybrid, and COLBT-hydro, parametric for SCETG). The I_{AA} is shown for $0-10\%$ Pb+Pb events for $p_T^Z > 60$ GeV. Figure from [45].

derprediction of the data. Several of these models also capture the relative difference in the I_{AA} between the three p_T^Z selections.

6. Summary

These proceedings summarize measurements of inclusive fragmentation functions measured as a function of jet p_T, charged particle p_T^{ch}, distance from the jet axis, rapidity of the jet, and collision centrality. Results for measurements of fragmentation functions in gamma-jet system and measurement of normalized charged particle yields in Z-jet system are also presented. Significant modifications of fragmentation pattern in Pb+Pb collisions with respect to pp collisions is quantified in details. Universal across measurements is the observed enhancement of soft particle production which increases with increasing distance from the jet axis, increasing jet momentum, and decreasing charged particle momentum. Results presented here should provide stringent constraints for theoretical modeling of jet quenching.

Acknowledgements

i. Copyright 2021 CERN for the benefit of the ATLAS Collaboration. Reproduction of this article or parts of it is allowed as specified in the CC-BY-4.0 license.

1. G. Roland, K. Safarik, and P. Steinberg. Heavy-ion collisions at the LHC. *Prog. Part. Nucl. Phys.* **77** (2014) 70.

2. Wit Busza, Krishna Rajagopal, andWilke van der Schee. Heavy Ion Collisions The Big Picture, and the Big Questions. *Ann. Rev. Nucl. Part. Sci.* **68** (2018) 339.

3. ATLAS Collaboration. The ATLAS Experiment at the CERN Large Hadron Collider. *JINST* **3** (2008) S08003.

4. ALICE Collaboration. Measurement of charged jet suppression in Pb-Pb collisions at $\sqrt{sNN}$ = 2.76 TeV. *JHEP*, **03** (2014) 013.

5. ATLAS Collaboration. Measurements of the Nuclear Modification Factor for Jets in Pb+Pb Collisions at $\sqrt{sNN}$ = 2.76 TeV with the ATLAS Detector. *Phys. Rev. Lett.*, **114** (2015) 072302.

6. ALICE Collaboration. Measurement of jet suppression in central Pb-Pb collisions at $\sqrt{sNN}$ = 2.76 TeV. *Phys. Lett. B*, **746** (2015) 1-14.

7. CMS Collaboration. Measurement of inclusive jet cross sections in pp and PbPb collisions at $\sqrt{sNN}$ = 2.76 TeV. *Phys. Rev. C*, **96** (2017) 015202.

8. ATLAS Collaboration. Measurement of the nuclear modification factor for inclusive jets in Pb+Pb collisions at $\sqrt{sNN}$= 5.02 TeV with the ATLAS detector. *Phys. Lett. B*, **790** (2019) 108.

9. S. Chatrchyan *et al.*, Studies of jet quenching using isolated-photon+jet correlations in PbPb and pp collisions at $\sqrt{sNN}$ = 2.76 TeV. *Phys. Lett. B*, **718** 773- (2013) 794.

10. ATLAS Collaboration. Measurement of photon-jet transverse momentum correlations in 5.02 TeV Pb+Pb and pp collisions with ATLAS. *Phys. Lett. B*, **789** (2019) 167.

11. ATLAS Collaboration. Observation of a Centrality- Dependent Dijet Asymmetry in Lead-Lead Collisions at $\sqrt{sNN}$ = 2.76 TeV with the ATLAS Detector at the LHC. *Phys. Rev. Lett.*, **105** (2010) 252303.

12. CMS Collaboration. Observation and studies of jet quenching in PbPb collisions at nucleon-nucleon centerof- mass energy = 2.76 TeV. *Phys. Rev. C*, **84** (2011) 024906.

13. ATLAS Collaboration. Measurement of jet pT correlations in Pb+Pb and pp collisions at $\sqrt{sNN}$ = 2.76 TeV with the ATLAS detector. *Phys. Lett. B*, **774** (2017) 379.

14. ATLAS Collaboration. Measurement of the jet fragmentation function and transverse profile in proton-proton collisions at a center-of-mass energy of 7 TeV with the ATLAS detector. *Eur. Phys. J. C*, **71** (2011) 1795.

15. ALICE Collaboration. Medium modification of the shape of small-radius jets in central Pb-Pb collisions at $\sqrt{sNN}$ = 2.76TeV. *JHEP*, **10** (2018) 139.

16. CMS Collaboration. Shape, Transverse Size, and Charged Hadron Multiplicity of Jets in pp Collisions at 7 TeV. *JHEP*, **06** (2012) 160.

17. CMS Collaboration. Modification of Jet Shapes in PbPb Collisions at $\sqrt{sNN}$ = 2.76 TeV. *Phys. Lett. B*, **730** (2014) 243.

18. CMS Collaboration. Measurement of transverse momentum relative to dijet systems in PbPb and pp collisions at $\sqrt{sNN}$ = 2.76 TeV. *JHEP*, **01** (2016) 006.

19. CMS Collaboration. Decomposing transverse momentum balance contributions for quenched jets in PbPb collisions at $\sqrt{sNN}$ = 2.76 TeV. *JHEP*, **11** (2016) 055.

20. CMS Collaboration. Jet properties in PbPb and pp collisions at $\sqrt{sNN}$ = 5.02 TeV. *JHEP*, **05** (2018) 006.

21. ALICE Collaboration. Measurement of jet radial profiles in Pb-Pb collisions at $\sqrt{sNN}$ = 2.76 TeV. *Phys. Lett. B*, **796** (2019) 204.

22. I. Vitev, SimonWicks, and B.-W. Zhang. A Theory of jet shapes and cross sections From hadrons to nuclei. *JHEP*, **11** (2008) 093.

23. G. Ovanesyan and I. Vitev. An effective theory for jet propagation in dense QCD matter jet broadening and medium-induced bremsstrahlung. *JHEP*, **06** (2011) 080.

24. J.-P. Blaizot, Y. Mehtar-Tani, and M. A. C. Torres. Angular structure of the in-medium QCD cascade. *Phys. Rev. Lett.*, **114** (2015) 222002.

25. G.-You Qin and X.-Nian Wang. Jet quenching in high-energy heavy-ion collisions. *Int. J. Mod. Phys. E*, **24** (2015) 1530014.

26. M. A. Escobedo and Edmond Iancu. Event-by-event fluctuations in the medium-induced jet evolution. *JHEP*, **05** (2016) 008.

27. J.Casalderrey-Solana, D. Gulhan, G. Milhano, D. Pablos, and K. Rajagopal. Angular Structure of Jet Quenching Within a Hybrid Strong/Weak Coupling Model. *JHEP*, **03** (2017) 135.

28. Y. Tachibana, N.-Bo Chang, and G.-You Qin, Full jet in quark-gluon plasma with hydrodynamic medium response. *Phys. Rev. C*, **95** (2017) 044909.

29. ATLAS Collaboration. Measurement of angular and momentum distributions of charged particles within and around jets in Pb+Pb and pp collisions at $\sqrt{sNN}$ = 5.02 TeV with the ATLAS detector. *Phys. Rev. C*, **100** (2019) 064901. [Erratum *Phys.Rev.C* **101** (2020) 059903].

30. Martin Spousta and Brian Cole. Interpreting single jet measurements in Pb + Pb collisions at the LHC. *Eur. Phys. J. C*, **76** (2016) 50.

31. ATLAS Collaboration. Centrality, rapidity and transverse momentum dependence of isolated prompt photon production in lead-lead collisions at $\sqrt{sNN}$ = 2.76 TeV measured with the ATLAS detector. *Phys. Rev. C*, **93** (2016) 034914.

32. ATLAS Collaboration. Measurement of photon-jet transverse momentum correlations in 5.02 TeV Pb + Pb and pp collisions with ATLAS. *Phys. Lett. B*, **789** (2019) 167.

33. CMS Collaboration. Study of jet quenching with isolated-photon+jet correlations in PbPb and pp collisions at $\sqrt{sNN}$ = 5.02 TeV. *Phys. Lett. B*, **785** (2018) 14.

34. J. Casalderrey-Solana, D. C. Gulhan, J. Guilherme Milhano, D. Pablos, and K. Rajagopal, Predictions for Boson-Jet Observables and Fragmentation Function Ratios from a Hybrid Strong/Weak Coupling Model for Jet Quenching. *JHEP*, **03** (2016) 053.

35. Zhong-Bo Kang, Ivan Vitev, and Hongxi Xing. Vectorboson-tagged jet production in heavy ion collisions at energies available at the CERN Large Hadron Collider. *Phys. Rev. C*, **96** (2017) 014912.

36. Raghav Kunnawalkam Elayavalli and Korinna Christine Zapp. Simulating V+jet processes in heavy ion collisions with JEWEL. *Eur. Phys. J. C*, **76** (2016) 695.

37. ATLAS Collaboration. Measurement of jet fragmentation in Pb+Pb and pp collisions at $\sqrt{sNN}$ = 2.76 TeV with the ATLAS detector at the LHC. *Eur. Phys. J. C*, **77** (2017) 379.

38. ATLAS Collaboration. Measurement of jet fragmentation in Pb+Pb and pp collisions at $\sqrt{sNN}$ = 5.02 TeV with the ATLAS detector. *Phys. Rev. C*, **98** (2018) 024908.

39. ATLAS Collaboration. Measurement of inclusive jet charged-particle fragmentation functions in Pb+Pb collisions at $\sqrt{sNN}$ = 2.76 TeV with the ATLAS detector. *Phys. Lett. B*, **739** (2014) 320.

40. ATLAS Collaboration. Comparison of Fragmentation Functions for Jets Dominated by Light Quarks and Gluons from pp and Pb+Pb Collisions in ATLAS. *Phys. Rev. Lett.*, **123** (2019) 042001.

41. ATLAS Collaboration. Measurement of Z boson Production in Pb+Pb Collisions at $\sqrt{sNN}$ = 2.76 TeV with the ATLAS Detector. *Phys. Rev. Lett.*, **110** (2013) 022301.

42. ATLAS Collaboration. Z boson production in Pb+Pb collisions at $\sqrt{sNN}$ = 5.02 TeV measured by the ATLAS experiment. *Phys. Lett. B*, **802** (2020) 135262.

43. V. Kartvelishvili, R. Kvatadze, and R. Shanidze. On Z and Z + jet production in heavy ion collisions. *Phys. Lett. B*. **356** (1995) 589.

44. R. B. Neufeld and I. Vitev. The Z0-tagged jet event asymmetry in heavy-ion collisions at the CERN Large Hadron Collider. *Phys. Rev. Lett.*, **108** (2012) 242001.

45. ATLAS Collaboration.

46. Hai Tao Li and Ivan Vitev. Jet charge modification in dense QCD matter. *Phys. Rev. D*, **101** (2020) 076020.

47. Yang-Ting Chien, Alexander Emerman, Zhong-Bo Kang, Grigory Ovanesyan, and Ivan Vitev. Jet Quenching from QCD Evolution. *Phys. Rev. D* **93** (2016) 074030.

48. W. Chen, Shanshan Cao, T. Luo, L.-G. Pang, and X.-Nian Wang, Effects of jet-induced medium excitation in γ-hadron correlation in A+A collisions. *Phys. Lett. B*, **777** (2018) 86.

49. Wei Chen, Shanshan Cao, Tan Luo, Long-Gang Pang, and Xin-NianWang. Medium modification of γ-jet fragmentation functions in Pb+Pb collisions at LHC. *Phys. Lett. B*, **810** (2020) 135783.